Article

Sorbent Properties of Orange Peel-Based Biochar for Different Pollutants in Water

Weichao Zhang, Yuwei Wang * , Liquan Fan *, Xingmei Liu, Weiyan Cao, Honglin Ai, Ziteng Wang, Xijun Liu and Hongge Jia

Heilongjiang Provincial Key Laboratory of Polymeric Composite Materials, College of Materials Science and Engineering, Qiqihar University, No. 42, Wenhua Street, Qiqihar 161006, China; zhang980502@163.com (W.Z.); lxm19980112@163.com (X.L.); weiyan19970606@163.com (W.C.); aihonglin2021@163.com (H.A.); wzt991202@163.com (Z.W.); liuxijun2002@163.com (X.L.); jiahongge@qqhru.edu.cn (H.J.)
* Correspondence: ywwang@qqhru.edu.cn (Y.W.); 02275@qqhru.edu.cn (L.F.)

Abstract: Efficient and reasonable utilization of waste biomass resources can not only avoid serious waste of material resources, but also solve the problem of environmental pollution. Therefore, the development of efficient and environmentally friendly waste biomass carbonization technology has important practical significance. Here, the activated carbon from orange peel (OAC) is prepared by potassium hydroxide (KOH) activation combined with high-temperature carbonization. The adsorption effects of OAC on three different pollutant aqueous solutions, methylene blue (MB), tetracycline (TC), and fluorescein sodium (NaFL), are examined. The OAC absorbent has excellent adsorption capacity for MB, TC, and NaFL pollutants of 10 mg L^{-1}, with adsorption rates of 99.17%, 73.5%, and 94.24%, respectively. This study provides a new idea for turning waste biomass into treasure and eliminating the hidden danger of environmental pollution.

Keywords: activated carbon; adsorption; dye; antibiotic

1. Introduction

To meet people's increasing demands for production and living, all kinds of industries such as paper making, textile, coating, and medical treatment have thrived, which have caused severe environmental pollution while promoting rapid economic development [1]. With the discharge of industrial wastes, pollutants such as toxic dyes and antibiotics directly enter various water sources, which not only destroy the ecological environment of aquatic organisms, but also cause immeasurable harm to human health and ecological systems [2]. Organic dyes not only hinder photosynthesis in aquatic ecosystems, but also cause carcinogenicity and mutagenicity in human bodies [3]. The introduction of methylene blue (MB) into the human body causes many adverse reactions [4]. Ingestion of specific doses of fluorescein sodium (NaFL) may irritate the stomach, and inhalation of luciferin sodium dust may cause respiratory symptoms. As the health care industry develops, the use of antibiotics continues to rise [5]. Tetracycline (TC) is a broad-spectrum antibiotic that inhibits bacterial protein synthesis, which is widely used to treat human diseases and prevent bacterial infections in livestock. Tetracycline can enter the environment through incomplete metabolism in humans or animals. Low concentrations of antibiotics in garbage and manure can spread into water environments and induce bacterial resistance to drugs, causing severe harm to human health and ecosystems [6]. Developing low-cost and efficient adsorbent-adsorbed water pollutants is a major approach in water pollution treatment.

In recent years, numerous studies have been undertaken about biomass carbon adsorbents [7]. Amongst them, biomass carbon prepared by pyrolysis under anaerobic or low oxygen conditions has a porous structure with highly specific surface area and large functional groups such as hydroxyl and carboxyl groups on the surface [8]. The physical and chemical properties of biomass are different due to the various raw materials and

pyrolysis processes [9]. As an essential adsorbent with apparent advantages, such as ease of scale-up, high cost-effectiveness, and environmental friendliness, biomass carbon has received increasing attention [10]. In addition, biomass carbon derived from agricultural waste can not only reduce the cost of raw materials, but also carry out efficient recovery and utilization of agricultural waste [11]. A large amount of biomass waste can be used to prepare adsorbents for absorbing pollutants in water. Zhang et al. [12] used the outer skin of mangosteen as a carbon source to prepare activated carbon (AC) with a large specific surface area. The AC showed good adsorption performance for MB, with adsorption capacity up to 871.49 mg g^{-1}. After three cycles, the treatment effect of MB can still reach more than 40%. The mangosteen peel AC has feasible applications for dyes removal. Prusov et al. [13] synthesized flax, shive-based AC through KOH activation and high-temperature pyrolysis, which showed an adsorption capacity of 464.2 mg g^{-1} for MB. The AC can be as an efficient adsorbent for wastewater purification. Araújo et al. [14] reported that palm endocarp biochar activated by $ZnCl_2$ was used for an adsorbent for MB. The adsorption capacity of MB reached 48~229.9 mg g^{-1} in the temperature range from 30 to 60 °C. The AC showed a promising MB removal performance. Yağmur et al. [15] reported the magnetic AC made of coconut shell as raw material and activated by $ZnCl_2$, followed by the Fe^{3+}/Fe^{2+} co-precipitation, gives a maximum adsorption capacity of 156.25 mg g^{-1} for MB. The low-cost magnetic AC may be used as the MB dye adsorbent. Gu et al. [16] synthesized porous carbon by combining cotton and polyester textile waste with shell as carbon source and obtained AC with a maximum adsorption capacity of 515.17 mg g^{-1} for TC. The low-cost AC is considered to be an effective adsorbent for TC adsorption. Zheng et al. [17] used sweet potato as biomass carbon source and a hydrothermal method to synthesize biochar for treating TC in wastewater. The maximum adsorption capacity of activated carbon on TC was 238.7 mg g^{-1}. The mesoporous AC is a highly efficient removal reagent of TC.

In this study, the orange peel was used as a carbon source to obtain biomass-activated carbon (OAC) by KOH activation and high-temperature carbonization. The adsorption capacities of OAC to MB, NaFL, and TC were examined.

2. Materials and Methods

2.1. Material Preparation

Tangerine peels are from leaf tangerines purchased in Wal-Mart supermarkets. Potassium hydroxide (GR95%), methylene blue, and sodium fluorescein (≥99.5%) are all purchased from Shanghai Aladdin Biochemical Technology Co., Ltd. (Shanghai, China) Tetracycline (≥99.5%) is supplied from Shanghai Makclin Biochemical Co., Ltd. (Shanghai, China) 10 mg L^{-1} of MB, NaFL, and TC solutions were prepared in ultrapure water.

The orange peels were washed with plenty of water and dried naturally to remove moisture. The samples were cut into small pieces, placed in a drying oven at 60 °C for 24 h, and then ground in a grinder to obtain the powder. The orange peel powder obtained above was placed in the quartz tube of a tubular furnace. It was first aired by N_2 for 20 min, then heated to 400 °C at a heating rate of 2.5 °C min^{-1}, and kept at 400 °C for 2 h under nitrogen atmosphere to obtain orange-peel-activated carbon (named OC).

An appropriate amount of OC powder was dissolved into KOH solutions with different concentrations of 6 mol L^{-1}, 7 mol L^{-1}, and 9 mol L^{-1}, respectively, and stirred for 6 h. The solution was then treated by ultrasonic at 80 °C for 2 h. The collected powder after filtration was placed in a drying oven at 60 °C and kept for 24 h. Nitrogen was introduced into the tubular furnace over 20 min to ensure the air was empty thoroughly. The samples were heated to 800 °C under a nitrogen atmosphere at 5 °C min^{-1} and kept at 800 °C for a period of 1 h. The pH value of these three samples was adjusted to 7 with 2 mol L^{-1} HCl. After drying at 60 °C for 24 h, the dried samples were denoted as OAC−6, OAC−7, and OAC−9, respectively, corresponding to the activation concentration of KOH.

2.2. Characterization of Adsorbents

The microstructure of all the samples was investigated with scanning electron microscopy (SEM, JSM-7410F, Tokyo, Japan, JEOL). Phases in the adsorbents were identified by X-ray diffraction (XRD, D8, Germany BRUKER-AXS). An N_2 desorption test was used to determine the specific surface area and pore size structure of the samples (BET, ASAP2020, Norcross, GA, USA, American Micromeritics Instrument Corporation). A Fourier transform infrared spectrometer was used to analyze the functional groups on the sample surface (FT-IR, Spectrum, PerkinElmer, Waltham, MA, USA). The chemical composition of the material surface was measured by X-ray photoelectron spectroscopy (XPS ESCALAB250Xi, Thermo Fisher Scientific, Waltham, MA, USA). The absorbance of pollutant aqueous solution was measured by ultraviolet spectrophotometer (UV-Vis-NIR, Lambda 750, PerkinElmer, Waltham, MA, USA). The absorption wavelengths of the three pollutant aqueous solutions are MB (664 nm), TC (360 nm), and NaFL (493 nm), respectively.

2.3. Adsorption Capacity Analysis

In this study, the adsorption equilibrium of three different types of pollutants, MB, TC and NaFL, was determined by porous carbon materials. The sample usage amount was 0.2 g, the volume of polluted water was 20 mL, and the pollutant concentration was 10 mg L^{-1}. The removal rate (R) (%) of the pollutants in the equilibrium state can be calculated by the following formula:

$$R(\%) = \frac{(C_0 - C_t)}{C_0} \times 100 \tag{1}$$

Among them, C_0 (mg g^{-1}) is the initial concentration and C_t (mg g^{-1}) is the concentration of the solution at a given time.

2.4. Adsorption Kinetic Model

The sample has been tested for adsorption kinetics. In the kinetic test, the adsorption capacity can be calculated by the following formula:

$$q_t = \frac{(C_0 - C_t)V}{W} \tag{2}$$

Among them, q_t (μg g^{-1}) is the adsorption amount of the sample to the pollutants. C_0 (μg L^{-1}) is the initial concentration; C_t (μg L^{-1}) is the concentration of the solution at a given time t. V (L) is the volume of the solution. W (g) is the mass of the sample.

The adsorption kinetics of activated carbon is usually simulated by pseudo-first [18] and pseudo-second [19] kinetic models.

The pseudo-first order adsorption kinetic equation is as follows:

$$\ln(q_e - q_t) = \ln(q_e) - k_1 t \tag{3}$$

Among them, q_e is the amount of adsorption at equilibrium (μg g^{-1}), q_t is the amount of adsorption at any moment (μg g^{-1}), and k_1 is the adsorption rate constant of the pseudo-first order kinetic equation (L min^{-1}).

The pseudo-second order adsorption kinetic equation is:

$$\frac{t}{q_t} = \frac{1}{k_2 q_e^2} + \frac{t}{q_e} \tag{4}$$

Among them, k_2 is the adsorption rate constant of the pseudo-second order kinetic equation [g (mg min^{-1})].

3. Results and Discussion

3.1. Characterization of Absorbents

The microstructures of OC, OAC−6, OAC−7, and OAC−9 were characterized using SEM analysis, as shown in Figure 1. As shown in Figure 1a, the surface of OC initially carbonized at 400 °C was relatively smooth, only showing the tubular channels of orange peel itself, and the pore size was large, which was not conducive to the adsorption of pollutants in water. After carbonization at 800 °C, the pore distribution on the OAC surface increases with KOH concentration. After carbonization at 800 °C, the pore distribution on the OAC surface increases with the increase of KOH concentration, as shown in Figure 1b–d. After 9M KOH treatment, the surface of OAC−9 has the most abundant pore structure.
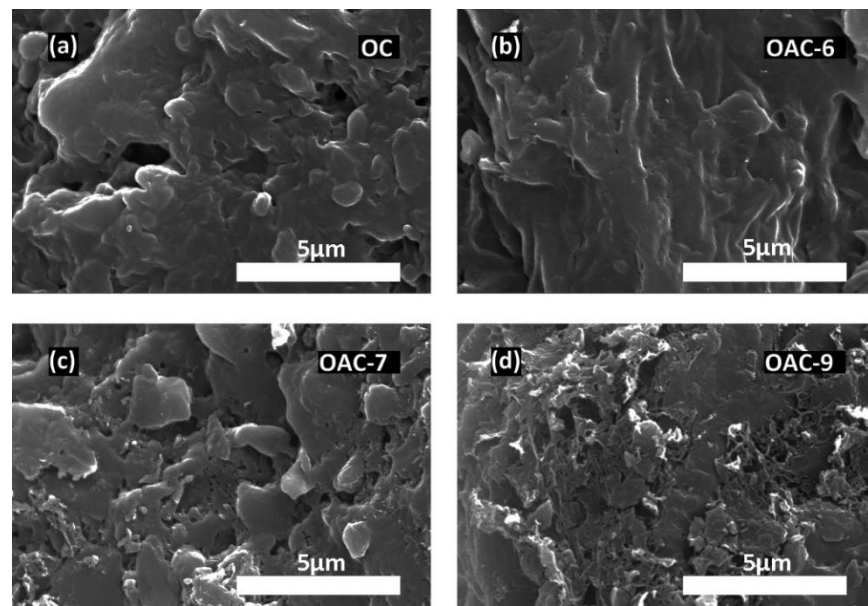
Figure 1. SEM images of (**a**) OC, (**b**) OAC-6, (**c**) OAC-7, and (**d**) OAC-9.

The crystal types of OC, OAC−6, OAC−7, and OAC−9 were tested by XRD. It can be seen in Figure 2 that the XRD patterns of the four materials are seriously broadened, indicating that all the samples have poor crystallinity and are primarily amorphous. The two broad peaks at 26° and 44° correspond to the (002) and (100) characteristic crystal planes of graphite, respectively, indicating that the four materials have been initially graphitized. The diffraction peak intensity of OAC−6, OAC−7, and OAC−9 is significantly stronger than that of OC, indicating that the higher temperature carbonization treatment can improve the graphitization degree of samples.
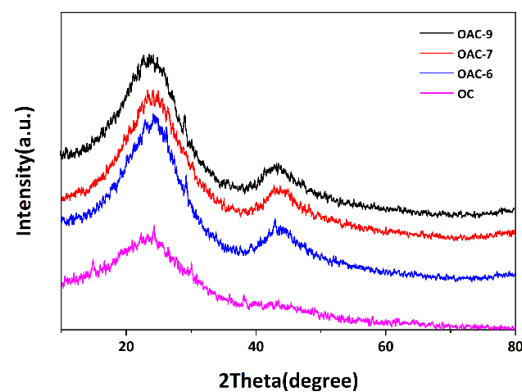
Figure 2. XRD patterns of OC, OAC−6, OAC−7, and OAC−9.

Figure 3 shows the N_2 adsorption/desorption isotherm and the pore-size distribution of the adsorbents, which are summarized in Table 1 in detail. Generally speaking, some substances in the carbon structure evaporate at high temperatures, increasing the specific surface area [20]. KOH and carbon generate K_2CO_3, which is pyrolyzed at a high temperature to generate carbon dioxide, resulting in pores in the carbon structure and increasing the defects of activated carbon.
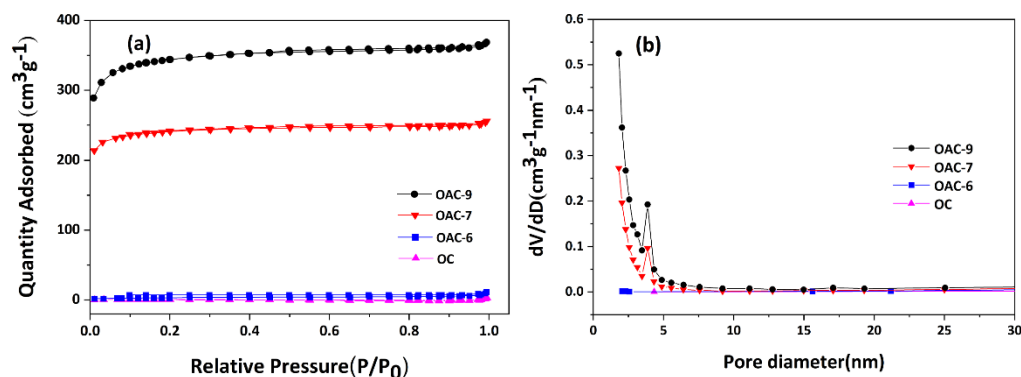
Figure 3. (**a**) N_2 sorption isotherms and (**b**) pore size distributions of OC, OAC$-$6, OAC$-$7, and OAC$-$9.

Table 1. N_2 sorption data and pore size data.

Sample	Specific Surface Area (m^2 g^{-1})	Aperture (nm)
OC	0.90	147.57
OAC-6	7.84	8.61
OAC-7	723.68	3.49
OAC-9	1046.51	3.30

The surface molecular structure of the adsorbents was examined by Fourier infrared spectroscopy (FT-IR), as shown in Figure 4. The diffraction peaks of C=O (1565 cm^{-1}), C-O (1043 cm^{-1}), -CH (862 cm^{-1}) O=C-O (1408 cm^{-1}), and -OH (3464 cm^{-1}) make the activated carbon have a certain physical and chemical adsorption capacity [21]. The functional group stretching vibration peak intensity of OAC$-$9 is stronger than OAC$-$7 and OAC$-$6, making the adsorption capacity of OAC$-$9 stronger than other samples.
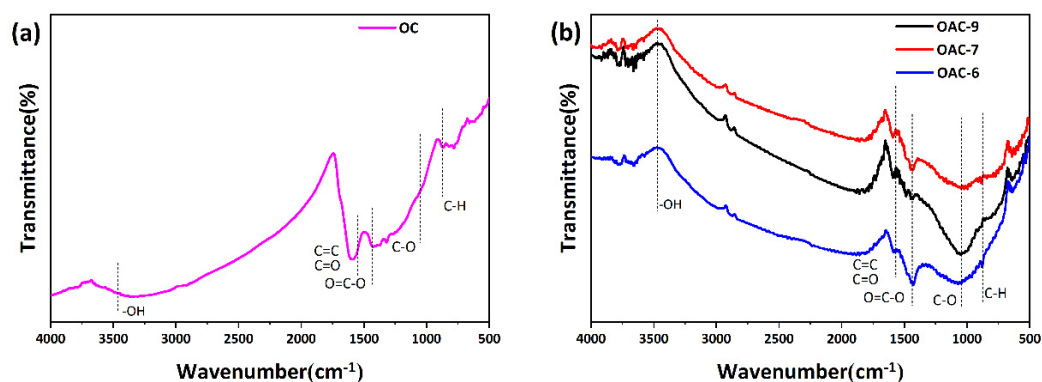
Figure 4. (**a**) FT-IR spectra of OC, and (**b**) FT-IR spectra of OAC$-$6, OAC$-$7, and OAC$-$9.

X-ray photoelectron spectroscopy (XPS) was used to characterize the elements contained in the adsorbents and the chemical states of the elements (Figure 5). Peaks of C and O were detected in all samples. These adsorbent materials all contain C and O elements. As shown in Figure 5b, the OAC$-$9 C1s spectrum exhibits four prominent peaks at 284.8,

285.5, 286.3, and 289.3 eV, which can be assigned to C-C, C-OH, C=O, and COOH [22], respectively. The species of reactive oxygen functional groups contained in these adsorbent materials were consistent with FI-TR test results. Figure 5c shows high-resolution O1s spectra of the adsorbents. Two characteristic peaks at 531.3 eV and 532.3 eV are attributed to C-OH and C=O functional groups, respectively. The surface of OAC contains a large number of hydroxyl and carboxyl functional groups, which is beneficial to produce good chemisorption of various polar organic compounds. The XPS element contents of OC, OAC−6, OAC−7, and OAC−9 are summarized in Table 2.
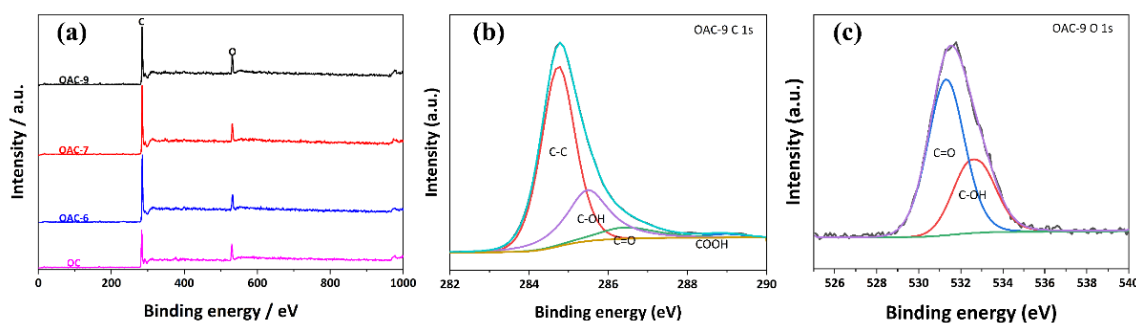
Figure 5. (**a**) Full-survey XPS spectra of OC, OAC−6, OAC−7, and OAC−9. High-resolution XPS spectra of (**b**) C 1s, (**c**) O 1s for OAC−9.

Table 2. XPS element content of OC, OAC−6, OAC−7, and OAC−9.

Sample	C (%)	O (%)
OC	80.80	14.54
OAC-6	87.05	10.80
OAC-7	88.94	10.06
OAC-9	84.78	11.32

3.2. Adsorption Performance of the Adsorbents

3.2.1. Adsorption Equilibrium

As shown in Figure 6, OAC−9 has the best adsorption effect on the three pollutants. In the MB solution, the adsorption rate of OAC−9 is up to 99.17%. In TC and NaFL solutions, the adsorption rates reach 73.50% and 94.24%, respectively. The reason why OAC-9 has excellent adsorption capacity is mainly due to the large specific surface area of OAC-9, which significantly improves the contact area between OAC−9 and the target pollutant. Moreover, the wealthy oxygen-containing functional groups on the surface of OAC-9 have a synergistic effect on the adsorption of contaminants.
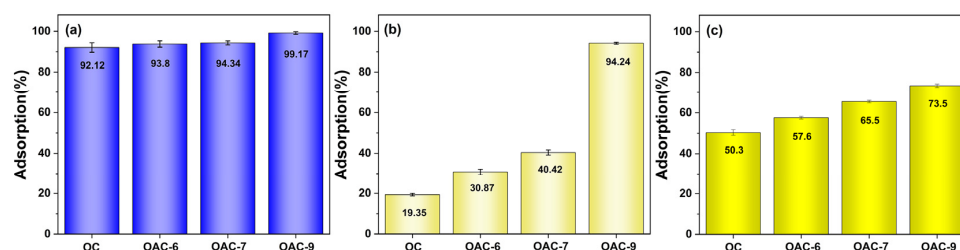
Figure 6. Adsorption equilibrium of the adsorbents for 10 mg L^{-1} of (**a**) MB, (**b**) NaFL, and (**c**) TC for a period of 2 h.

3.2.2. Adsorption Rate

Figure 7 shows the adsorption kinetic properties of OC, OAC−6, OAC−7, and OAC−9 for MB, TC, and NaFL pollutants in water. All the adsorbent samples can achieve fast adsorption of the target substance; the adsorption rate is very fast in the first 20 min and the

adsorption equilibrium can be reached within 30 min. By contrast, OAC-9 has the highest adsorption rates of 99.17%, 73.5%, and 94.24% for MB, OC, and FL, respectively.
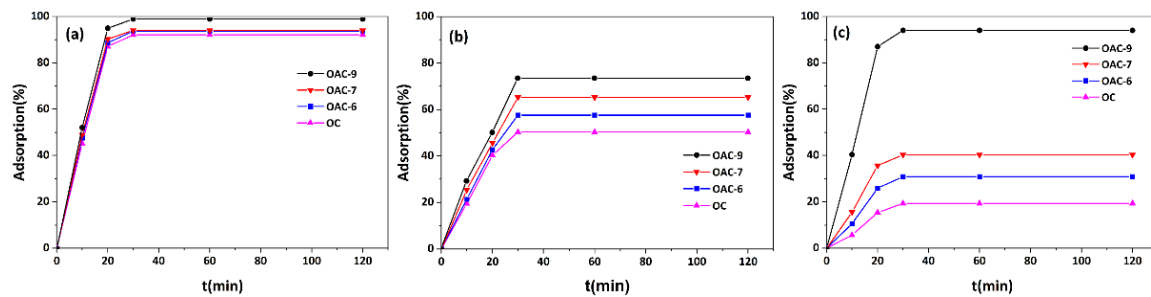
Figure 7. Adsorption rates of the adsorbents for 10 mg L^{-1} of (**a**) MB, (**b**) TC, and (**c**) NaFL.

3.2.3. Adsorption Kinetics

The pseudo-first order and pseudo-second order kinetic models are used to fit the adsorption kinetic data and to compare them, in order to provide insights into the adsorption mechanism. In general, the initial state of the reaction process, especially the initial state of fast adsorption, is more in line with the pseudo-first order kinetic model [18]. However, the pseudo-second order kinetic model is consistent with long-term adsorption with chemical adsorption as a rate-controlled process [19]. Figure 8 shows the simulation results of the first and second order kinetic models for the adsorption of MB, TC, and NaFL by four activated carbon materials. From Figure 8a–c, it can be seen that the actual adsorption data has a high degree of fit with the linear expression of the first-order kinetics. This result is consistent with the results shown in Table 3, indicating that the first-order kinetic model is more in line with the activity carbon adsorption kinetic model.

Table 3. Kinetic parameters of the pseudo-first-order models and pseudo-second-order models for MB, TC, and NaFL adsorption to the carbonaceous materials.

	OC	OAC−6	OAC−7	OAC−9
MB				
q_e (µg g^{-1})	921	938	943	992
First-order kinetic model				
k_1 (min^{-1})	0.146	0.144	0.161	0.160
R_2	0.971	0.975	0.975	0.976
Second-order kinetic model				
k_2 [g (mg min)$^{-1}$]	1.052	1.100	0.791	0.827
R_2	0.939	0.944	0.944	0.945
TC				
q_e (µg g^{-1})	503	576	655	735
First-order kinetic model				
k_1 (min^{-1})	0.081	0.068	0.060	0.058
R_2	0.968	0.967	0.970	0.969
Second-order kinetic model				
k_2 [g (mg min)$^{-1}$]	2.500	4.020	5.594	6.865
R_2	0.935	0.935	0.941	0.941
NaFL				
q_e (µg g^{-1})	193	308	404	942
First-order kinetic model				
k_1 (min^{-1})	0.080	0.092	0.109	0.131
R_2	0.942	0.952	0.957	0.960
Second-order kinetic model				
k_2 [g (mg h)$^{-1}$]	0.977	1.165	1.038	1.490
R_2	0.905	0.915	0.921	0.925
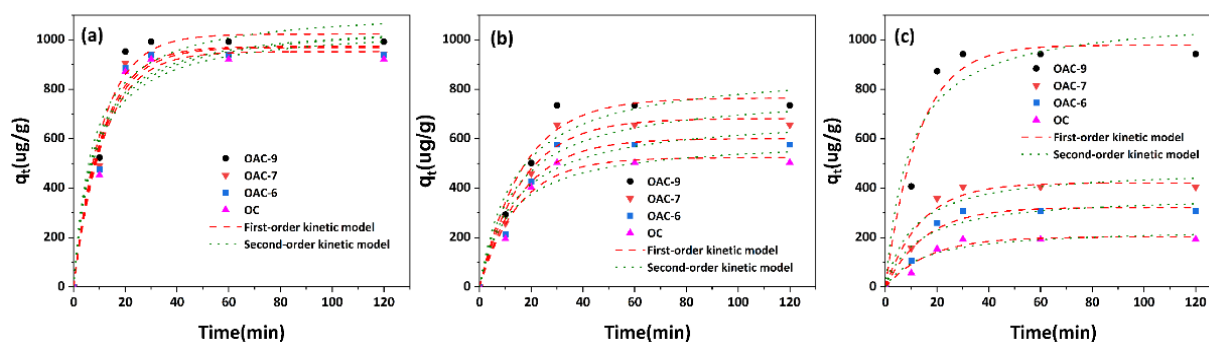
Figure 8. Adsorption kinetic of the adsorbents for 10 mg L^{-1} of (**a**) MB, (**b**) TC, and (**c**) NaFL.

3.2.4. Regeneration of Adsorbents

The adsorbent should not only have high adsorption capacity, but also have recycling and regeneration capacity. If the adsorbent can be reused under the premise of achieving the desired adsorption effect, the preparation cost of the adsorbent will be significantly reduced. Here, the adsorption cycle experiment of MB was carried out by using OAC−9. Methanol and glacial acetic acid with the volume ratio of 9:1 were used as the eluent for OAC−9 after adsorption. After five times of adsorption and desorption, the adsorption effect of OAC−9 on 10 mg L^{-1} MB decreased slightly, with a value of 82.34%, which still has a high adsorption efficiency (see Figure 9). The decrease in the adsorption efficiency of OAC−9 may be due to the adsorption of MB by OAC−9. MB molecules block part of the active adsorption sites of the micropores and are a challenge to be eluted by the eluent. In addition, due to the mass loss of OAC−9 during elution, the adsorption effect is reduced. Therefore, the reuse of OAC−9 needs to be further improved [23].
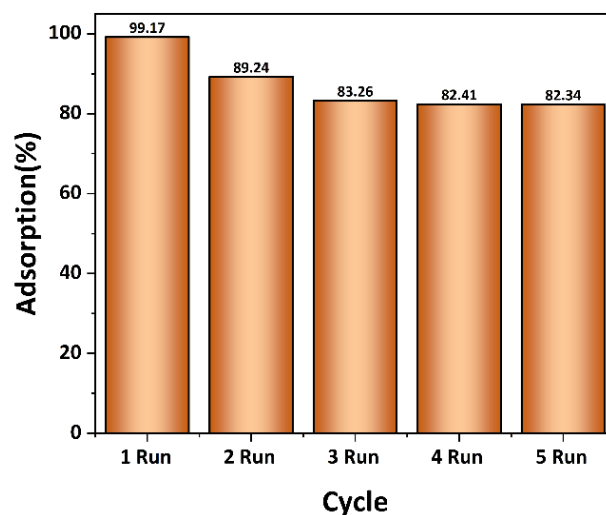
Figure 9. Reusability study of OAC−9 on MB adsorption.

3.2.5. Adsorption Mechanism and Comparison of Adsorption Properties

The most abundant mesoporous structure, graphite crystals, and hydroxyl and carboxyl functional groups of OAC−9 result in high adsorption capability. The pseudo-first order models were well-matched to the adsorption data. For the sake of comparison, the adsorption rates of some biomass-based activated carbon reported in the literature are summarized in Table 4. The adsorption rates of OAC−9 for MB, TC, and NaFL pollutants reach 99.17%, 73.5%, and 94.24%, respectively, which is close to or superior to comparable reported values [23–28].

Table 4. Comparison of adsorption properties of biomass-based activated carbon reported in literature.

Raw Material	Activating Agent	Processing Conditions	Specific Surface Area	Adsorbed Pollutants and Dosage	Adsorption Time	Adsorption Rate (%)	Ref.
Mandarin peel	NaOH	4 h 105 °C		MB and MO (1, 3, 5, 10, 30 mg L^{-1})	180 min	MB: 99.77% MO: 79.87%	[23]
Orange peel	ZnCl$_2$	800 °C	1439.50 m^2 g^{-1}	MB (0, 50, 100, 200, 400, 700, and 1100 mg L^{-1})	24 h	99%	[24]
Green pea peels	H$_2$SO$_4$	30 min 800 °C	316.20 m^2 g^{-1}	MB (50, 100, 150, and 200 mg L^{-1})	10 h	96–89.73%	[25]
Jack fruit peel	NaOH	0.5 h 700 °C	1286.7 m^2 g^{-1}	MB (1000 mg L^{-1})	25 h	80%	[26]
Apricot nut shells	H$_3$PO$_4$	90 min 400 °C	307.6 m^2 g^{-1}	TC (100 mg L^{-1})	24 h	98%	[27]
Sugar cane bagasse	ZnCl$_2$	120 min 600 °C	831.23 m^2 g^{-1}	TC (120–240 mg L^{-1})	20 h	96%	[28]
Orange peel	KOH	1 h 800 °C	1046 m^2 g^{-1}	MB, TC and NaFL (10 mg L^{-1})	30 min	MB: 99.17% TC: 73.5% NaFL: 94.24%	This work

4. Conclusions

The waste biomass resources in the world are extremely rich, but the utilization rate of the waste biomass all over the world is very low, which not only causes the serious waste of biomass resources, but also intensifies the pollution or potential pollution to the environment. Biomass carbonization technology is a new technology of biomass resource utilization. It is of great significance to make full use of waste biomass to treat the pollutants in water to relieve the pressure caused by energy shortages, ecological imbalances, environmental pollution, and other problems.

In this study, a series of activated carbon materials were prepared by using cheap and readily available orange peel as raw material. OAC−9 treated with a high concentration of KOH and high-temperature carbonization has the best adsorption effect on the three target pollutant solutions, 10 mg L^{-1} of MB, TC, and NaFL. OAC−9 contains many oxygen-containing functional groups (O=C-O, -OH), which makes it have a strong polarity adsorption capacity. The adsorption efficiency of MB, TC, and NaFL reaches 99.17%, 73.5%, and 94.24%, respectively. OAC−9 has a rapid adsorption capacity and can quickly reach adsorption peak and equilibrium within 20–30 min. OAC−9 can be used as an efficient and low-cost activated carbon adsorbent for various dyes and antibiotic contaminants in water.

Author Contributions: Conceptualization, W.Z. and L.F.; methodology, Y.W.; formal analysis, W.Z. and Y.W.; investigation, W.Z. and Y.W.; writing—original draft preparation, W.Z.; writing—review and editing, L.F. and X.L. (Xingmei Liu); visualization, W.C., H.A. and Z.W.; supervision, X.L. (Xijun Liu) and H.J.; project administration, Y.W., L.F. and W.Z.; funding acquisition, Y.W. and W.Z. All authors have read and agreed to the published version of the manuscript.

Institutional Review Board Statement: Not applicable.

Informed Consent Statement: Not applicable.

Data Availability Statement: Data contained within the article and additional materials are available on request from the authors.

Conflicts of Interest: The authors declare no conflict of interest.

References

1. Madeira, J.G.F.; Oliveira, E.M.; Springer, M.V.; Cabral, H.L.; do Barbeito, D.F.C.; Souza, A.P.G.; da Moura, D.A.S.; Delgado, A.R.S. Hydrogen production from swine manure biogas via steam reforming of methane (SRM) and water gas shift (WGS): A ecological, technical, and economic analysis. *Int. J. Hydrogen Energy* **2021**, *46*, 8961–8971. [CrossRef]
2. Singla, S.; Sharma, S.; Basu, S.; Shetti, N.P.; Aminabhavi, T.M. Photocatalytic water splitting hydrogen production via environmental benign carbon based nanomaterials. *Int. J. Hydrogen Energy* **2021**, *46*, 33696–33717. [CrossRef]
3. Ramsay, R.R.; Dunford, C.; Gillman, P.K. Methylene blue and serotonin toxicity: Inhibition of monoamine oxidase A (MAO A) confirms a theoretical prediction: Methylene blue inhibits monoamine oxidase A. *Br. J. Pharmacol.* **2007**, *152*, 946–951. [CrossRef] [PubMed]
4. Hejtmancik, M.R. Hematological effects in F344 rats and B6C3F1 mice during the 13-week gavage toxicity study of methylene blue trihydrate. *Toxicol. Sci.* **2002**, *65*, 126–134. [CrossRef] [PubMed]
5. Yang, J.-F.; Ying, G.-G.; Zhou, L.-J.; Liu, S.; Zhao, J.-L. Dissipation of oxytetracycline in soils under different redox conditions. *Environ. Pollut.* **2009**, *157*, 2704–2709. [CrossRef] [PubMed]
6. Chen, H.; Yan, T.; Jiang, F. Adsorption of Cr(VI) from aqueous solution on mesoporous carbon nitride. *J. Taiwan Inst. Chem. Eng.* **2014**, *45*, 1842–1849. [CrossRef]
7. Wei, D.; Li, B.; Huang, H.; Luo, L.; Zhang, J.; Yang, Y.; Guo, J.; Tang, L.; Zeng, G.; Zhou, Y. Biochar-based functional materials in the purification of agricultural wastewater: Fabrication, application and future research needs. *Chemosphere* **2018**, *197*, 165–180. [CrossRef] [PubMed]
8. Kong, X.; Liu, Y.; Pi, J.; Li, W.; Liao, Q.; Shang, J. Low-cost magnetic herbal biochar: Characterization and application for antibiotic removal. *Environ. Sci. Pollut. Res.* **2017**, *24*, 6679–6687. [CrossRef]
9. Tomczyk, A.; Sokołowska, Z.; Boguta, P. Biochar physicochemical properties: Pyrolysis temperature and feedstock kind effects. *Rev. Environ. Sci. Biotechnol.* **2020**, *19*, 191–215. [CrossRef]
10. Babel, S. Low-cost adsorbents for heavy metals uptake from contaminated water: A review. *J. Hazard. Mater.* **2003**, *97*, 219–243. [CrossRef]
11. Babel, S.; Kurniawan, T.A. Cr(VI) removal from synthetic wastewater using coconut shell charcoal and commercial activated carbon modified with oxidizing agents and/or chitosan. *Chemosphere* **2004**, *54*, 951–967. [CrossRef]
12. Zhang, Z.; Xu, L.; Liu, Y.; Feng, R.; Zou, T.; Zhang, Y.; Kang, Y.; Zhou, P. Efficient removal of methylene blue using the mesoporous activated carbon obtained from mangosteen peel wastes: Kinetic, equilibrium, and thermodynamic studies. *Microporous Mesoporous Mater.* **2021**, *315*, 110904. [CrossRef]
13. Prusov, A.N.; Prusova, S.M.; Radugin, M.V.; Bazanov, A.V. Flax shive as a source of activated carbon for adsorption of methylene blue. *Fuller. Nanotub. Carbon Nanostruct.* **2021**, *29*, 685–694. [CrossRef]
14. Araújo, L.K.F.; Albuquerque, A.A.; Ramos, W.C.O.; Santos, A.T.; Carvalho, S.H.V.; Soletti, J.I.; Bispo, M.D. Elaeis guineensis-activated carbon for methylene blue removal: Adsorption capacity and optimization using CCD-RSM. *Environ. Dev. Sustain.* **2021**, *23*, 11732–11750. [CrossRef]
15. Yağmur, H.K.; Kaya, İ. Synthesis and characterization of magnetic $ZnCl_2$-activated carbon produced from coconut shell for the adsorption of methylene blue. *J. Mol. Struct.* **2021**, *1232*, 130071. [CrossRef]
16. Gu, S.; Zhang, D.; Gao, Y.; Qi, R.; Chen, W.; Xu, Z. Fabrication of porous carbon derived from cotton/polyester waste mixed with oyster shells: Pore-forming process and application for tetracycline removal. *Chemosphere* **2021**, *270*, 129483. [CrossRef]
17. Zheng, Z.; Zhao, B.; Guo, Y.; Guo, Y.; Pak, T.; Li, G. Preparation of mesoporous batatas biochar via soft-template method for high efficiency removal of tetracycline. *Sci. Total Environ.* **2021**, *787*, 147397. [CrossRef]
18. Ho, Y.S.; McKay, G. A Comparison of Chemisorption Kinetic Models Applied to Pollutant Removal on Various Sorbents. *Process Saf. Environ. Prot.* **1998**, *76*, 332–340. [CrossRef]
19. Ho, Y.S.; McKay, G. Pseudo-second order model for sorption processes. *Process Biochem.* **1999**, *34*, 451–465. [CrossRef]
20. Xiao, L.; Bi, E.; Du, B.; Zhao, X.; Xing, C. Surface characterization of maize-straw-derived biochars and their sorption performance for MTBE and benzene. *Environ. Earth Sci.* **2014**, *71*, 5195–5205. [CrossRef]
21. Ahmad, M.; Lee, S.S.; Dou, X.; Mohan, D.; Sung, J.-K.; Yang, J.E.; Ok, Y.S. Effects of pyrolysis temperature on soybean stover- and peanut shell-derived biochar properties and TCE adsorption in water. *Bioresour. Technol.* **2012**, *118*, 536–544. [CrossRef] [PubMed]
22. Stankovich, S.; Dikin, D.A.; Piner, R.D.; Kohlhaas, K.A.; Kleinhammes, A.; Jia, Y.; Wu, Y.; Nguyen, S.T.; Ruoff, R.S. Synthesis of graphene-based nanosheets via chemical reduction of exfoliated graphite oxide. *Carbon* **2007**, *45*, 1558–1565. [CrossRef]
23. Unugul, T.; Nigiz, F.U. Preparation and Characterization an Active Carbon Adsorbent from Waste Mandarin Peel and Determination of Adsorption Behavior on Removal of Synthetic Dye Solutions. *Water Air. Soil Pollut.* **2020**, *231*, 538. [CrossRef]
24. Bediako, J.K.; Lin, S.; Sarkar, A.K.; Zhao, Y.; Choi, J.-W.; Song, M.-H.; Cho, C.-W.; Yun, Y.-S. Evaluation of orange peel-derived activated carbons for treatment of dye-contaminated wastewater tailings. *Environ. Sci. Pollut. Res.* **2020**, *27*, 1053–1068. [CrossRef]

25. Dod, R.; Banerjee, G.; Saini, S. Adsorption of methylene blue using green pea peels (Pisum sativum): A cost-effective option for dye-based wastewater treatment. *Biotechnol. Bioprocess Eng.* **2012**, *17*, 862–874. [CrossRef]

26. Foo, K.Y.; Hameed, B.H. Potential of jackfruit peel as precursor for activated carbon prepared by microwave induced NaOH activation. *Bioresour. Technol.* **2012**, *112*, 143–150. [CrossRef]

27. Marzbali, M.H.; Esmaieli, M.; Abolghasemi, H.; Marzbali, M.H. Tetracycline adsorption by H_3PO_4-activated carbon produced from apricot nut shells: A batch study. *Process Saf. Environ. Prot.* **2016**, *102*, 700–709. [CrossRef]

28. Cai, Y.; Liu, L.; Tian, H.; Yang, Z.; Luo, X. Adsorption and desorption performance and mechanism of tetracycline hydrochloride by activated carbon-based adsorbents derived from sugar cane bagasse activated with $ZnCl_2$. *Molecules* **2019**, *24*, 4534. [CrossRef]